

Political Optimizer with Deep Learning-Enabled Tongue Color Image Analysis Model

Anwer Mustafa Hilal^{1,*}, Eatedal Alabdulkreem², Jaber S. Alzahrani³, Majdy M. Eltahir⁴, Mohamed I. Eldesouki⁵, Ishfaq Yaseen¹, Abdelwahed Motwakel¹ and Radwa Marzouk⁶

¹Department of Computer and Self Development, Preparatory Year Deanship, Prince Sattam bin Abdulaziz University, AlKharj, Saudi Arabia

²Department of Computer Sciences, College of Computer and Information Sciences, Princess Nourah bint Abdulrahman University, P.O. Box 84428, Riyadh, 11671, Saudi Arabia

³Department of Industrial Engineering, College of Engineering at Alqunfudah, Umm Al-Qura University, Mecca, 24382, Saudi Arabia

⁴Department of Information Systems, College of Science & Art at Mahayil, King Khalid University, Abha, 62529, Saudi Arabia

⁵Department of Information System, College of Computer Engineering and Sciences, Prince Sattam bin Abdulaziz University, AlKharj, Saudi Arabia

⁶Department of Mathematics, Faculty of Science, Cairo University, Giza, 12613, Egypt

*Corresponding Author: Anwer Mustafa Hilal. Email: a.hilal@psau.edu.sa

Received: 17 March 2022; Accepted: 26 April 2022

Abstract: Biomedical image processing is widely utilized for disease detection and classification of biomedical images. Tongue color image analysis is an effective and non-invasive tool for carrying out secondary detection at anytime and anywhere. For removing the qualitative aspect, tongue images are quantitatively inspected, proposing a novel disease classification model in an automated way is preferable. This article introduces a novel political optimizer with deep learning enabled tongue color image analysis (PODL-TCIA) technique. The presented PODL-TCIA model purposes to detect the occurrence of the disease by examining the color of the tongue. To attain this, the PODL-TCIA model initially performs image pre-processing to enhance medical image quality. Followed by, Inception with ResNet-v2 model is employed for feature extraction. Besides, political optimizer (PO) with twin support vector machine (TSVM) model is exploited for image classification process, shows the novelty of the work. The design of PO algorithm assists in the optimal parameter selection of the TSVM model. For ensuring the enhanced outcomes of the PODL-TCIA model, a wide-ranging experimental analysis was applied and the outcomes reported the betterment of the PODL-TCIA model over the recent approaches.

Keywords: Tongue color image analysis; political optimizer; twin support vector machine; inception model; deep learning

1 Introduction

Tongue diagnosis is a productive painless strategy for assessing the condition of an individual's inside parts in oriental prescription, i.e., Japanese conventional herbal medication, traditional Chinese medication



This work is licensed under a Creative Commons Attribution 4.0 International License, which permits unrestricted use, distribution, and reproduction in any medium, provided the original work is properly cited.

(TCM), etc [1,2]. Traditionally, restorative doctors will examine these color features relying on broad information. Be that as it may, subjectivity and equivocalness are frequently followed with their determinations result [3]. For eliminating these subjective elements, tongue color examinations are impartially inspected by their color features that give an original strategy to diagnosing infection, one that lessens the actual injury caused to individual (connected with another therapeutic examination). The analysis method depends on expert's view as indicated by visual assessment including structure, substance, color, movement, and covering the tongue [4]. As opposed to tongue irregular events and infection, regular tongue analyze are exceptionally energetic for perceiving the illness. For example, the tongue covering white oily and yellow thick event demonstrates hot and cold conditions, correspondingly that are associated with wellbeing states like safe, aggravation, contamination, endocrine, or stress problems. Eliminating the reliance on experience and emotional based examination of tongue analyses could altogether increase the chance of utilizing tongue analysis on the planet including Western medication [5]. Automated tongue appraisal including color adjustment, light assessment, image examination, math investigation, tongue division, etc can be a proficient gadget to analyze sickness that targets tending to this problem [6].

However, a few modules are relying on approach of individual features are introduced and accomplished compelling results, this sort of strategy utilizes lower level features [7]. It can be expected for coordinating a design which could make entire features from tongue images [8,9]. Hence, more significant level features have been expected for computer aided diagnosis (CAD) tongue investigations. In the current distributions was characterized and utilized deep learning (DL) methods for separating more significant level portrayals to broad vision investigation processes like article acknowledgment, transcribed digit recognizable proof, and face acknowledgment [10].

Mansou et al. [11] develop automatic Internet of Things (IoT) and synergic DL based tongue color images (ASDL-TCI) for disease classification and diagnosis. Furthermore, deep neural network (DNN) based classification is employed to define the presence of the disease. At last, enhanced black widow optimization (EBWO) related parameter tuning procedure was performed for improving the diagnosis accuracy. Jiang et al. [12] proposed an approach-based computer tongue image analysis technique for observing the tongue features of 1778 participants. Integrating basic information, serological indexes, and quantitative tongue image features. The applications of computer intelligent tongue diagnoses technique increase the performance of Non-alcoholic fatty liver disease (NAFLD) diagnoses and offer an appropriate methodological reference for the formation of earlier screening metho.

Yan et al. [13] developed a differentiable weighted histogram system for extracting color features that are utilized in a novel upsampling model named the mixed feature attention upsampling model for assisting image generation. In [14], the authors developed a computer aided smart decision support system, the DenseNet architecture is applied for identifying the essential feature of the tongue images namely texture, color, red spots, fur coating, and tooth markings. To implement Support Vector Machines (SVM) is applied for optimizing accuracy the SVM parameter is tuned via Particle Swarm Optimization (PSO) method. In [15], the authors proposed a stochastic region pooling technique for gaining comprehensive regional characteristics. As well, we proposed an inner-imaging channel relation modelling technique to model multiple region relationships on every network. Furthermore, it combines with the spatial attention module.

This article introduces a novel political optimizer with deep learning enabled tongue color image analysis (PODL-TCIA) approach. The presented PODL-TCIA model aims to detect the occurrence of the disease by examining the color of the tongue. To attain this, the PODL-TCIA model initially performs image pre-processing to enhance medical image quality. Followed by, Inception with ResNet-v2 model is employed for feature extraction. Besides, political optimizer (PO) with twin support vector machine (TSVM) model is exploited for image classification process. The design of PO algorithm assists in the

optimal parameter selection of the TSVM model. For ensuring the enhanced outcomes of the PODL-TCIA model, a wide-ranging experimental analysis is performed and the outcomes reported the betterment of the PODL-TCIA model over the recent approaches.

2 The Proposed Model

In this study, a novel PODL-TCIA model was established for the investigation of tongue color images. The presented PODL-TCIA model performed image pre-processing to improvise the quality of the medical images. Besides, the Inception with ResNet-v2 model is employed for feature extraction. Moreover, the PO with TSVM model is exploited for image classification process. Fig. 1 illustrates the overall block diagram of PODL-TCIA technique.

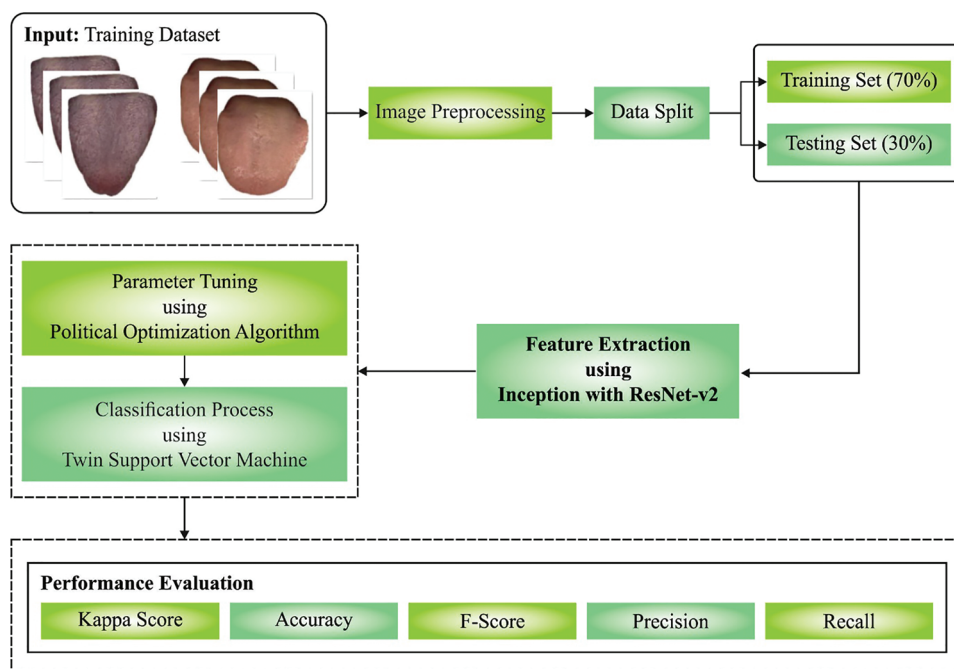


Figure 1: Block diagram of PODL-TCIA technique

2.1 Stage 1: Image Pre-processing

Primarily, the presented PODL-TCIA model performed image pre-processing to improvise the quality of the medical images. The median filter (MF) is used to remove the noise. For an image with null average noise in uniform distribution, the noise variant of the MF technique can be defined as follows.

$$\sigma_{med}^2 = \frac{1}{4nf^2(\bar{n})} \approx \frac{\sigma_i^2}{n + \frac{\pi}{2} - 1} \cdot \frac{\pi}{2}. \quad (1)$$

where σ_i^2 denotes input noise power, n implies MF neighborhood, $f(\bar{n})$ indicates noise density function. Based on noise variance, the mean filter can be defined as follows:

$$\sigma_0^2 = \frac{1}{n} \sigma_i^2. \quad (2)$$

2.2 Stage 2: Feature Extraction

Followed by, the Inception with ResNet-v2 model is employed for feature extraction [16]. Rather than developing a convolutional neural network (CNN) structure from scratch, the presented method is depending upon finetuning some topmost layers where weight in earlier layer is frozen. An earlier layer of CNN-based model is accountable to extract lower-level features, namely blobs, edges, lines, and so on. The effective extraction of this lower-level feature is very significant for image classification challenges. As pretrained deep CNN structure weight is highly previously enhanced on a huge data, the presented technique is depending on the finetuning of topmost layer to augment higher-level features when maintaining first layer frozen. Pretrained InceptionResNet-V2, depending on inception network and contains 164 layers. It incorporates residual connection as in ResNet architecture to improve the accuracy with lower computation cost. Afterward the summary of residual connection, batch normalization is included by all the blocks. To alleviate the training procedure, residual connection is scaled-down beforehand feeding into the activation of preceding layer. Fig. 2 depicts the structure of Inception ResNet v2. Here, the topmost two blocks of this technique are finetuned, and weight is upgraded. Global average pooling layer is employed, and the last 4 fully connected layers using 128, 1024, 512, and 256 units, correspondingly, as well as rectified linear unit (ReLU) activation is employed. For the final layer, the sigmoid activation function is utilized for binary classification.

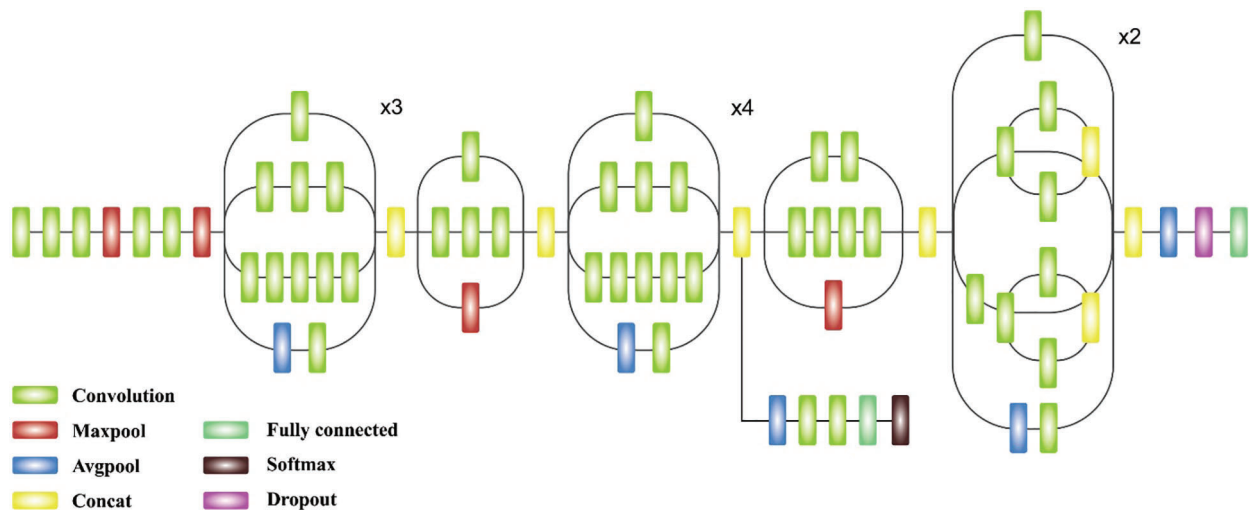


Figure 2: Inception ResNet v2

2.3 Stage 3: Hyperparameter Optimization

For optimal adjustment of the hyperparameters involved in the Inception with ResNet-v2 model, the PO algorithm has been employed to it. In PO technique is an existing meta-heuristic algorithm can be inspired by the political model with multi-phase nature [17]. The politics were dependent upon the political struggle amongst 2 individuals, all individual's attempts for improving their concern for winning the election. Each party attempts for expanding the count of seats from parliament to the highest range to procedure the government. In PO, the member of parties was regarded as a (candidate solution) if the individual concern was assumed as the individual place (design variable). The election refers the main function, for instance, defined based on the count of votes reached by candidates. The party development, parliamentary affairs, PO, party switching, electioneering, distribution of constituencies, and elections in the party are the 5 steps of the parliament. A primary phase was implemented one time, it can be regarded as initiation procedure once the other stages are applied from the loop.

During the party distribution step, the population includes n parties, every party has n member (candidate), and every member is defined as a d -dimensional vector. It could be stated mathematically as:

$$P = \{P_1, P_2, P_3, \dots, P_n\} \tag{3}$$

$$P_i = \{p_i^1, p_i^2, p_i^3, \dots, p_i^n\} \tag{4}$$

$$p_i^j = [p_{i,1}^j, p_{i,2}^j, p_{i,3}^j, \dots, p_n^j]^T \tag{5}$$

whereas P_n denotes the n^{th} political party and p_i^n signifies the n^{th} member. Besides, there are n precincts, each party candidate contest the election in the precinct as follows:

$$c = \{c_1, c_2, c_3, c_n\} \tag{6}$$

$$c_j = \{p_1^j, p_2^j, p_3^j, \dots, p_n^j\} \tag{7}$$

The fittest party member has been regarded as the leader, it could broadcast then the election inside the party as:

$$q = \arg \min f(p_i^j), \forall i \in \{1, 2, \dots, n\} \\ p_i^* = p_i^q \tag{8}$$

Assume p_i^* be the i^{th} party leader and $f(p_i^j)$ signifies the fitness function (FF) of p_i^j . The vector implies all the leaders are expressed as:

$$P^* = \{p_1^*, p_2^*, p_3^*, \dots, p_n^*\} \tag{9}$$

The vector of all parliamentarian is written as:

$$c^* = \{c_1^*, c_2^*, c_3^*, c_n^*\} \tag{10}$$

But c_j^* signifies the j^{th} constituency winner. The electioneering stage permits the candidate for improving its performance from the electoral process, it could be executed by 3 features are comparative analysis with winner, learning in the prior election, and effect of vote bank which the party leader reached. A primary one has been modeled by method of upgrade prior place as:

$$p_{i,k}^j(t+1) = \begin{cases} m^* + r(m^* - p_{i,k}^j(t)), & p_{i,k}^j(t-1) \leq p_{i,k}^j(t) \leq m^* \text{ or } p_{i,k}^j(t-1) \geq p_{i,k}^j(t) \geq m^* \\ m^* + (2r-1)|m^* - p_{i,k}^j(t)|, & p_{i,k}^j(t-1) \leq m^* \leq p_{i,k}^j(t) \text{ or } p_{i,k}^j(t-1) \geq m^* \geq p_{i,k}^j(t) \\ m^* + (2r-1)|m^* - p_{i,k}^j(t-1)|, & m^* \leq p_{i,k}^j(t-1) \leq p_{i,k}^j(t) \text{ or } m^* \geq p_{i,k}^j(t-1) \geq p_{i,k}^j(t) \end{cases} \tag{11}$$

$$p_{i,k}^j(t+1) = \begin{cases} m^* + (2r-1)|m^* - p_{i,k}^j(t)|, & p_{i,k}^j(t-1) \leq p_{i,k}^j(t) \leq m^* \text{ or } p_{i,k}^j(t-1) \geq p_{i,k}^j(t) \geq m^* \\ p_{i,k}^j(t-1) + r(p_{i,k}^j(t) - p_{i,k}^j(t-1)), & p_{i,k}^j(t-1) \leq m^* \leq p_{i,k}^j(t) \text{ or } p_{i,k}^j(t-1) \geq m^* \geq p_{i,k}^j(t) \\ m^* + (2r-1)|m^* - p_{i,k}^j(t-1)|, & m^* \leq p_{i,k}^j(t-1) \leq p_{i,k}^j(t) \text{ or } m^* \geq p_{i,k}^j(t-1) \geq p_{i,k}^j(t) \end{cases} \tag{12}$$

while r signifies the arbitrary number in zero and one, $p_{i,k}^j(t)$ denotes the place of j^{th} candidate of j^{th} political party at t iteration, and m^* refers the k dimension vector hold p_i^* and acts on c_j^* . The above formulas were executed to upgrade the candidate place based on the connections amongst the existing FF and prior one. Although the FF was improved once it can be placed when the fitness was degraded.

The party switching phase is executed by distributing a variable termed as party switch rate (λ), it introduced by λ_{\max} and linearly decreased to 0 at the time of iteration procedure. Every member is a possibility value of λ dependent upon the switching to (p_r^j) arbitrary party that is executed, the member is replaced as the worse fit member (p_r^q). The q index was evaluated as:

$$q = \operatorname{argmax}_f(p_r^j), \quad 1 \leq j \leq n \quad (13)$$

The Election was simulated by measuring the fitness of all individual's competing candidates from the electoral region and declaring the winner based on the succeeding formula:

$$q = \operatorname{argmin}_f(p_i^j), \forall i \in \{1, 2, \dots, n\} \quad (14)$$

$$c_j^* = p_i^q$$

whereas c_j^* signifies the j^{th} constituency winner, the party leader was upgraded by Eq. (14).

Then, executing the election inside the party, the government was generated. The parliamentarian was described. During this phase, the parliamentarians upgrade their place but the evaluated FF values were optimized.

2.4 Stage 4: Image Classification

At the final stage, the TSVM model has been executed for determining appropriate class labels to the tongue color images. The TWSVM is further progress of SVM projected [18]. TWSVM drives to find 2 symmetry planes for every plane takes a distance of approximately one data class and to probable in other data classes. Consider that trained data set D that holds a group of m row vector from n dimension space, $D = \{(x_i, y_i) | x_i \in X^m, y_i \in \{-1, +1\}, i = 1, 2, \dots, N\}$ and $y_i \in \{+1, -1\}$ signifies the class to that i^{th} instance goes to. Then, there are d_1 datapoints in class +1 and d_2 datapoint in class -1 so as $d_1 + d_2 = d$. It could be processed ($d_1 \times n$) matrix A that is datapoints in class +1, and ($d_2 \times n$) matrix B which is the datapoint in class -1. The 2 non-parallel hyperplanes are:

$$x^T w_1 + b_1 = 0 \quad (15)$$

$$x^T w_2 + b_2 = 0 \quad (16)$$

In which x signifies the data vector, w_1 implies the weighted parameter to primary hyperplane, b_1 defines the bias parameter to primary hyperplane, w_2 denotes the weighted parameter to 2nd hyperplane, and b_2 stands for the bias parameter to 2nd hyperplane. The TWSVM approach has been reached with resolve the following pair of quadratic programming problems:

TWSVM 1:

$$\min_{w_1, b_1, \xi_2} \frac{1}{2} \|Aw_1 + e_1 b_1\|^2 + c_1 e_2^T \xi_2 \quad (17)$$

subject to

$$-(Bw_1 + e_2b_1) \geq e_2 - \xi_2 \tag{18}$$

$$\xi_2 \geq 0 \tag{19}$$

and

TWSVM 2:

$$\min_{w_2, b_2, \xi_1} \frac{1}{2} \|Bw_2 + e_2b_2\|^2 + c_2 e_1^T \xi_1 \tag{20}$$

subject to

$$-(Aw_2 + e_2b_2) \geq e_1 - \xi_1 \tag{21}$$

$$\xi_1 \geq 0 \tag{22}$$

whereas $c_1 > 0$ and $c_2 > 0$ signifies the penalty parameters, ξ_1 and ξ_2 represents the slack variables, and e_1 and e_2 denotes the vectors of ones, i.e., every element has ‘one’ only.

The 2 hyperplanes of TWSVM with kernel:

$$K(x^T, C^T)u_1 + b_1 = 0 \tag{23}$$

$$K(x^T, C^T)u_2 + b_2 = 0 \tag{24}$$

In which $C^T = [A, B]^T$, $u_1, u_2 \in R^d$, and K stand for the kernel matrix corresponding to appropriately chosen kernel functions. The kernel TWSVM has been reached with solving the optimizing problem:

KTWSVM 1:

$$\min_{w_1, b_1, \xi_2} \frac{1}{2} \|K(A, C^T)u_1 + e_1b_1\|^2 + c_1 e_2^T \xi_2 \tag{25}$$

subject to

$$-(K(B, C^T)u_1 + e_2b_1) \geq e_2 - \xi_2 \tag{26}$$

$$\xi_2 \geq 0 \tag{27}$$

and

KTWSVM 2:

$$\min_{w_2, b_2, \xi_1} \frac{1}{2} \|K(B, C^T)u_2 + e_2b_2\|^2 + c_2 e_1^T \xi_1 \tag{28}$$

subject to

$$-(K(A, C^T)u_2 + e_2b_2) \geq e_1 - \xi_1 \tag{29}$$

$$\xi_1 \geq 0 \tag{30}$$

whereas $c_1 > 0$ and $c_2 > 0$ determines the penalty parameters, ξ_1 and ξ_2 defines the slack variables, e_1 and e_2 signifies the vectors of ‘ones’, i.e., every element is ‘one’ only, $C^T = [A, B]^T$, $u_1, u_2 \in R^d$, and K represent the kernel matrix equal to appropriately chosen kernel function.

3 Experimental Validation

This section investigates the enhanced performance of the PODL-TCIA model using tongue image dataset. The dataset comprises five classes with 50 images under each class. Fig. 3 depicts the sample images.



Figure 3: Sample images

Tab. 1 and Fig. 4 highlight the overall classification outcomes of the PODL-TCIA model on 70% of training phase. The obtained results indicated that the PODL-TCIA model has offered higher outcomes under all classes. For sample, under class 1, the PODL-TCIA model has provided $accu_y$, $prec_n$, $reca_l$, and F_{score} of 99.43%, 96.55%, 100%, and 98.25% respectively. Meanwhile, under class 2, the PODL-TCIA approach has provided $accu_y$, $prec_n$, $reca_l$, and F_{score} of 97.71%, 94.29%, 94.29%, and 94.29% correspondingly. Eventually, under class 3, the PODL-TCIA algorithm has provided $accu_y$, $prec_n$, $reca_l$, and F_{score} of 97.14%, 94.74%, 92.31%, and 93.51% correspondingly. Finally, under class 5, the PODL-TCIA methodology has provided $accu_y$, $prec_n$, $reca_l$, and F_{score} of 98.86%, 97.37%, 97.37%, and 97.37% respectively.

Table 1: Result analysis of PODL-TCIA technique under 70% of training dataset

| Class labels | Training phase (70%) | | | | |
|--------------|----------------------|-----------|--------|---------|-------------|
| | Accuracy | Precision | Recall | F-score | Kappa score |
| Class-1 | 99.43 | 96.55 | 100.00 | 98.25 | – |
| Class-2 | 97.71 | 94.29 | 94.29 | 94.29 | – |
| Class-3 | 97.14 | 94.74 | 92.31 | 93.51 | – |
| Class-4 | 100.00 | 100.00 | 100.00 | 100.00 | – |
| Class-5 | 98.86 | 97.37 | 97.37 | 97.37 | – |
| Average | 98.63 | 96.59 | 96.79 | 96.68 | 95.70 |

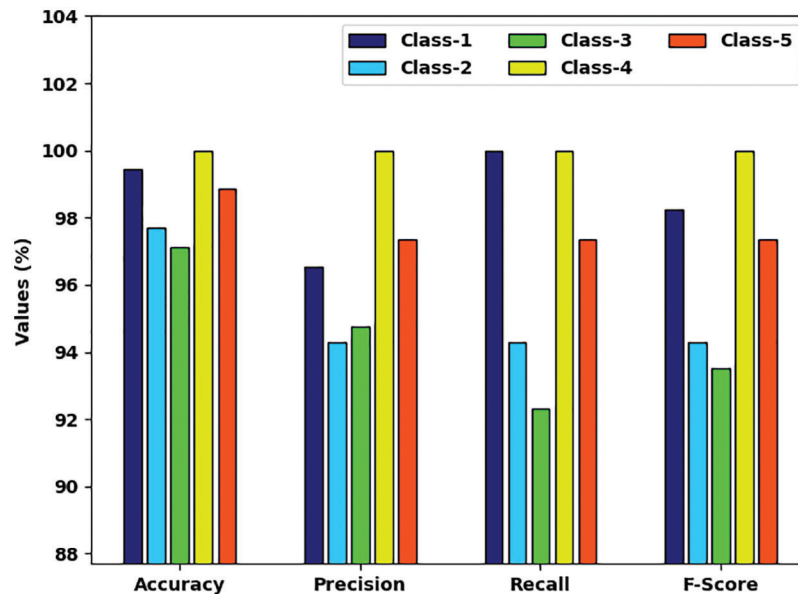


Figure 4: Result analysis of PODL-TCIA technique under 70% of training dataset

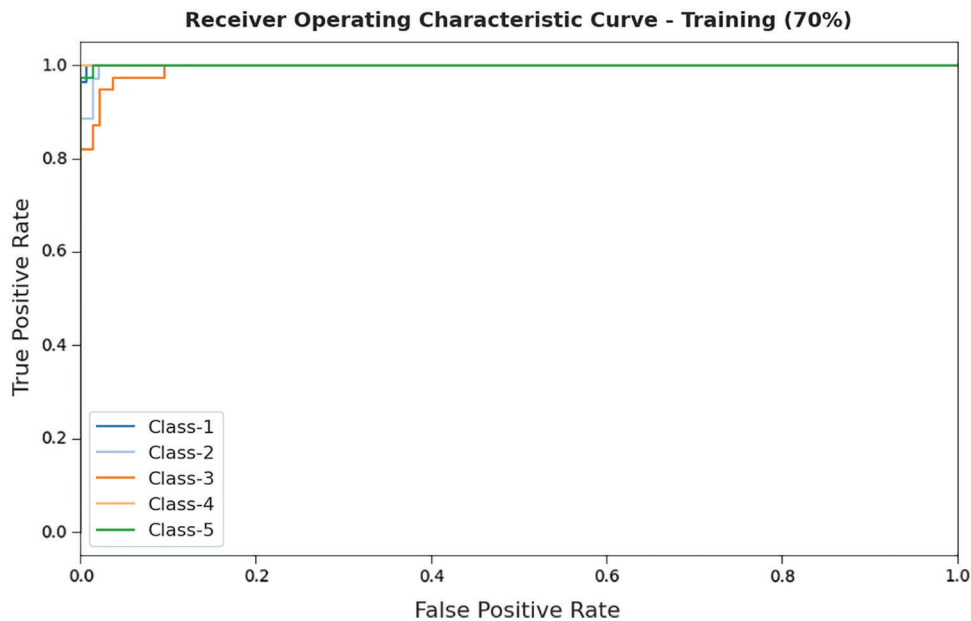


Figure 5: ROC analysis of PODL-TCIA technique under 70% of training dataset

A detailed ROC investigation of the PODL-TCIA model on 70% of training dataset is portrayed in Fig. 5. The results indicated that the PODL-TCIA model has exhibited its ability in categorizing five different classes on 70% of training dataset.

Tab. 2 and Fig. 6 highlights the overall classification outcomes of the PODL-TCIA technique on 30% of testing phase. The obtained results indicated that the PODL-TCIA methodology has offered higher outcomes under all classes. For sample, under class 1, the PODL-TCIA model has provided $accu_y$, $prec_n$, $reca_l$, and F_{score} of 98.67%, 100%, 95.45%, and 97.67% correspondingly. Also, under class 2, the PODL-TCIA

approach has provided $accu_y$, $prec_n$, $reca_l$, and F_{score} of 98.67%, 93.75%, 100%, and 96.77% correspondingly. At the same time, under class 3, the PODL-TCIA system has provided $accu_y$, $prec_n$, $reca_l$, and F_{score} of 98.67%, 91.67%, 100%, and 95.65% correspondingly. Lastly, under class 5, the PODL-TCIA approach has provided $accu_y$, $prec_n$, $reca_l$, and F_{score} of 98.67%, 100%, 91.67%, and 95.65% correspondingly.

Table 2: Result analysis of PODL-TCIA technique under 30% of testing dataset

| Testing phase (30%) | | | | | |
|---------------------|----------|-----------|--------|---------|-------------|
| Class labels | Accuracy | Precision | Recall | F-score | Kappa score |
| Class-1 | 98.67 | 100.00 | 95.45 | 97.67 | – |
| Class-2 | 98.67 | 93.75 | 100.00 | 96.77 | – |
| Class-3 | 98.67 | 91.67 | 100.00 | 95.65 | – |
| Class-4 | 100.00 | 100.00 | 100.00 | 100.00 | – |
| Class-5 | 98.67 | 100.00 | 91.67 | 95.65 | – |
| Average | 98.93 | 97.08 | 97.42 | 97.15 | 96.62 |

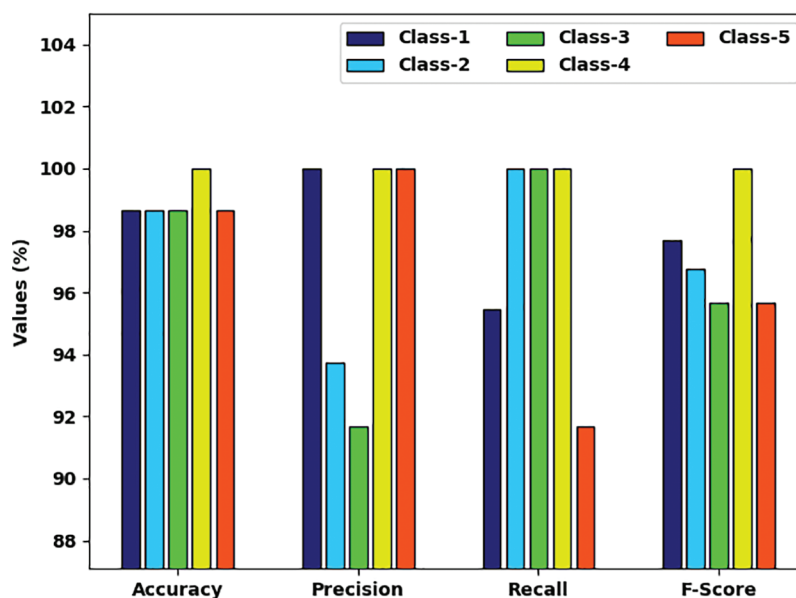


Figure 6: Result analysis of PODL-TCIA technique under 30% of testing dataset

A comprehensive Receiver operating characteristic (ROC) investigation of the PODL-TCIA model on 30% of testing dataset is portrayed in Fig. 7. The results designated that the PODL-TCIA model has exhibited its ability in categorizing five distinct classes on 30% of testing dataset.

Fig. 8 showcases the training and validation accuracy inspection of the PODL-TCIA approach on applied dataset. The figure conveyed that the PODL-TCIA technique has offered maximal training/validation accuracy on classification process.

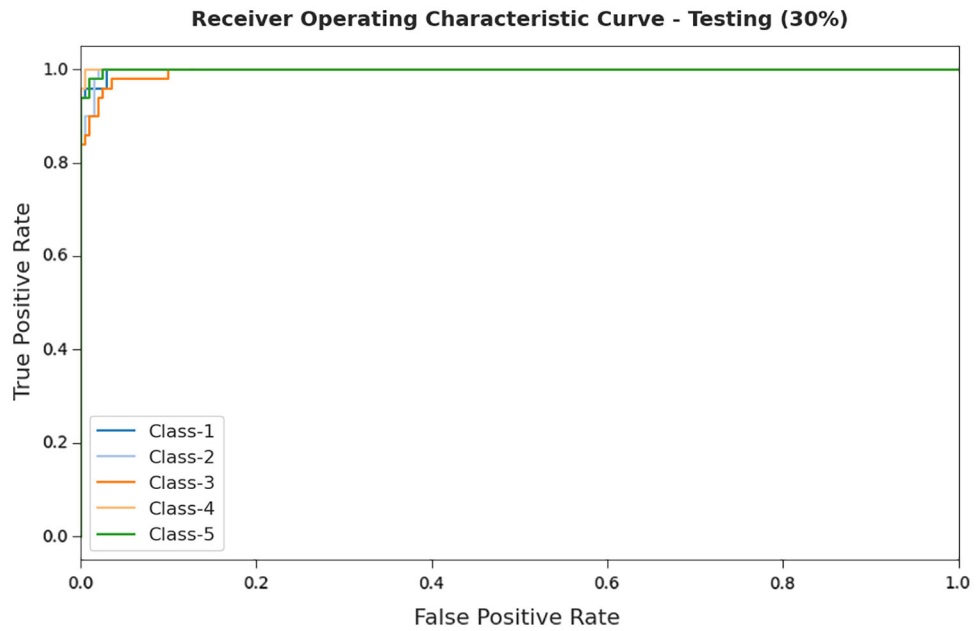


Figure 7: ROC analysis of PODL-TCIA technique under 30% of testing dataset

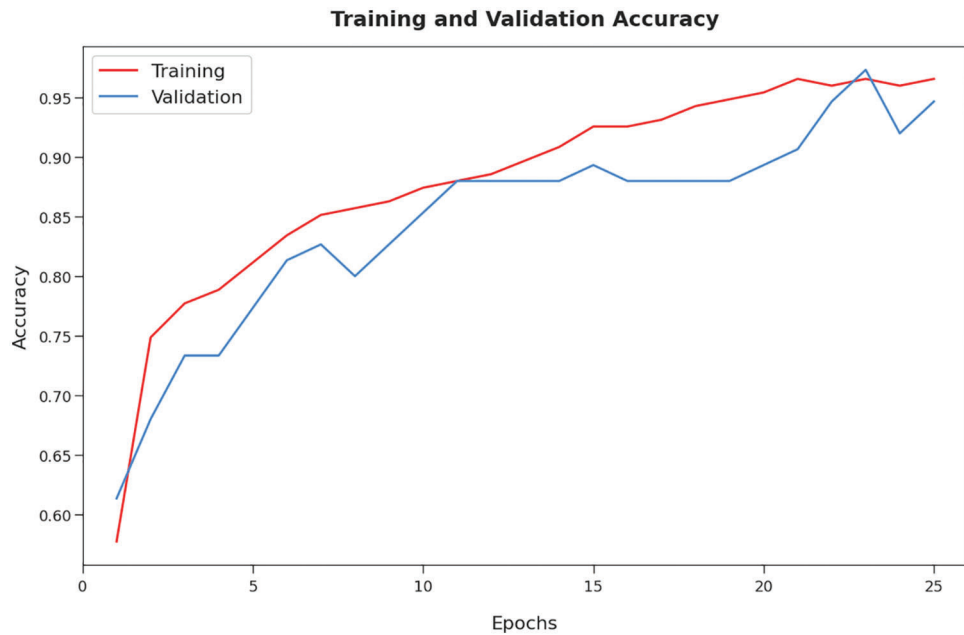


Figure 8: Accuracy graph analysis of PODL-TCIA technique

Next, [Fig. 9](#) demonstrates the training and validation loss inspection of the PODL-TCIA model on applied dataset. The figure reported that the PODL-TCIA method has offered reduced training/accuracy loss on the classification process of test data.

A comparative study of the PODL-TCIA model with other models is made in [Tab. 3](#).

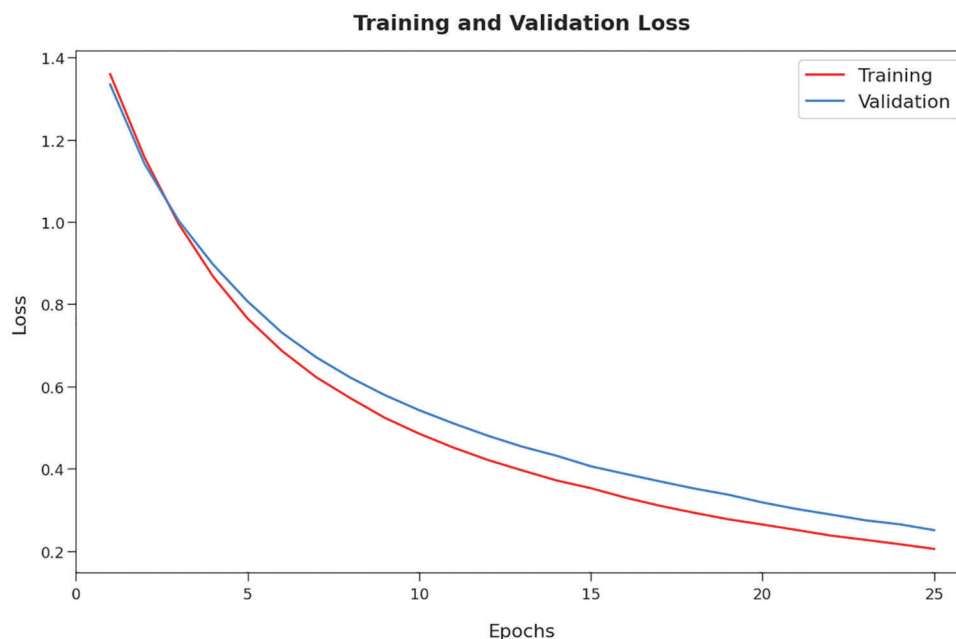


Figure 9: Loss graph analysis of PODL-TCIA technique

Table 3: Comparative analysis of PODL-TCIA method with existing algorithm

| Methods | Precision | Recall | Accuracy | F1-score | Kappa |
|--------------------|-----------|--------|----------|----------|-------|
| ASDL algorithm | 96.46 | 96.57 | 98.24 | 96.78 | 96.16 |
| SIFT-decision tree | 83.06 | 82.72 | 82.93 | 81.51 | 82.25 |
| HOG-decision tree | 89.25 | 89.24 | 89.72 | 88.43 | 87.70 |
| CNN-RF | 93.48 | 93.95 | 92.87 | 94.08 | 92.67 |
| CNN-GNB | 94.43 | 92.37 | 92.89 | 92.22 | 91.35 |
| PODL-TCIA | 97.08 | 97.42 | 98.93 | 97.15 | 96.62 |

Fig. 10 showcases a brief $accu_y$ examination of the PODL-TCIA model with other models. The figure indicated that the Scale-invariant feature transform (SIFT)-Decision Tree model has gained lower $accu_y$ value. In line with, the histogram of gradients (HOG)-Decision Tree model has resulted in slightly improved $accu_y$ value. Followed by, the CNN-random forest (RF) and CNN-Gaussian Naive Bayes (GNB) model has gained moderately closer $accu_y$ values. Though the ASDL model has resulted in reasonable increased $accu_y$ of 98.24% the PODL-TCIA model has accomplished maximum $accu_y$ of 98.93%.

Fig. 11 demonstrates a brief $prec_n$ and $reca_l$ examination of the PODL-TCIA model with other models. The figure indicated that the SIFT-Decision Tree approach has gained lower $prec_n$ and $reca_l$ value. Likewise, the HOG-Decision Tree model has resulted in slightly improved $prec_n$ and $reca_l$ value. Followed by, the CNN-RF and CNN-GNB model has gained moderately closer $prec_n$ and $reca_l$ values. But, the ASDL model has resulted in reasonable increased $prec_n$ and $reca_l$ of 96.46% and 96.57%, the PODL-TCIA model has accomplished maximal $prec_n$ and $reca_l$ of 97.08% and 97.42%.

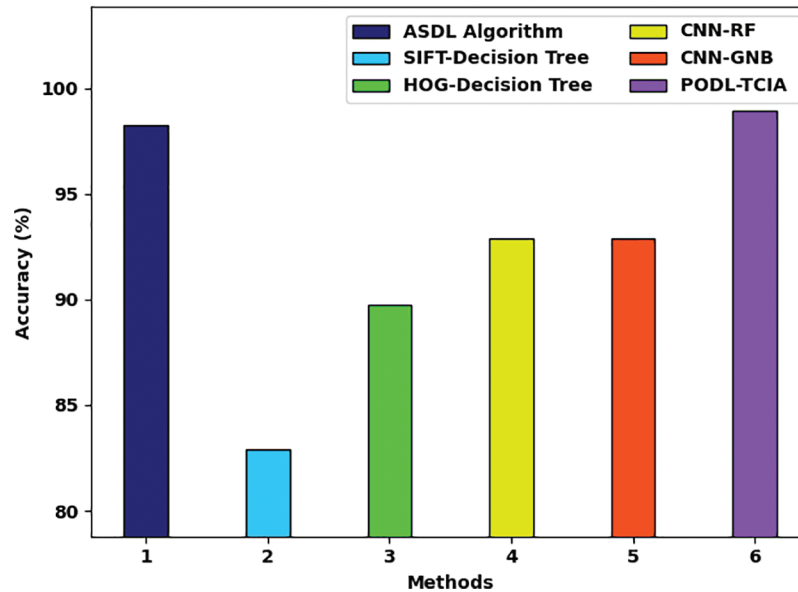


Figure 10: Acc_y analysis of PODL-TCIA algorithm with existing methods

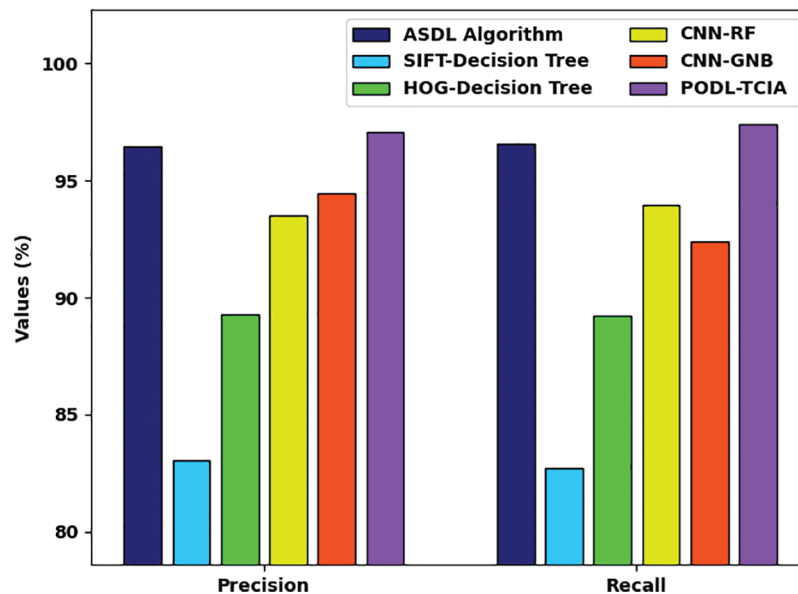


Figure 11: $Prec_n$ and $reca_l$ analysis of PODL-TCIA algorithm with existing methodologies

Fig. 12 illustrates a brief $F1_{score}$ and kappa examination of the PODL-TCIA model with other models [19]. The figure indicated that the SIFT-Decision Tree model has gained lower $F1_{score}$ and kappa value. Also, the HOG-Decision Tree model has resulted in slightly higher $F1_{score}$ and kappa value. Next, the CNN-RF and CNN-GNB model has gained moderately closer $F1_{score}$ and kappa values. Followed by the ASDL model has resulted in reasonable increased $F1_{score}$ and kappa of 96.78% and 96.16% the PODL-TCIA model has accomplished maximum $F1_{score}$ and kappa of 97.15% and 96.62%.

After noticing the detailed results, it is verified that the PODL-TCIA model is appropriate for tongue color image analysis.

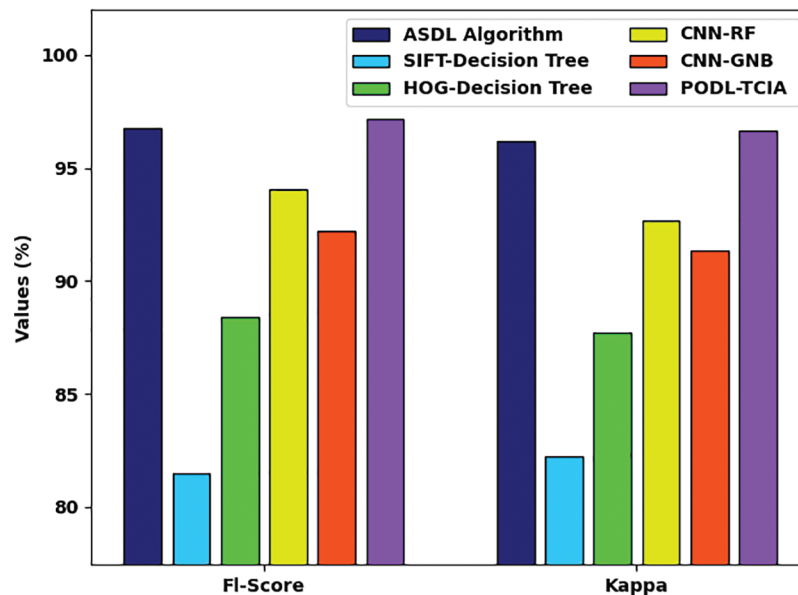


Figure 12: $F1_{score}$ and kappa analysis of PODL-TCIA algorithm with existing methods

4 Conclusion

In this study, a novel PODL-TCIA model was established for the investigation of tongue color images. The presented PODL-TCIA model performed image pre-processing to improve the quality of the medical images. Besides, the Inception with ResNet-v2 model is employed for feature extraction. Moreover, the PO with TSVM model is exploited for image classification process. The design of PO algorithm assists in the optimal parameter selection of the TSVM model. For ensuring the enhanced outcomes of the PODL-TCIA model, a wide-ranging experimental analysis is performed and the outcomes reported the betterment of the PODL-TCIA model over the recent approaches. Therefore, the PODL-TCIA model has been developed as an appropriate tool for tongue color image analysis. In future, hybrid DL models can be employed for improved results.

Funding Statement: The authors extend their appreciation to the Deanship of Scientific Research at King Khalid University for funding this work under grant number (RGP 2/158/43). Princess Nourah bint Abdulrahman University Researchers Supporting Project number (PNURSP2022R161), Princess Nourah bint Abdulrahman University, Riyadh, Saudi Arabia. The authors would like to thank the Deanship of Scientific Research at Umm Al-Qura University for supporting this work by Grant Code: (22UQU4340237DSR11).

Conflicts of Interest: The authors declare that they have no conflicts of interest to report regarding the present study.

References

- [1] J. Li, Q. Chen, X. Hu, P. Yuan, L. Cui *et al.*, "Establishment of noninvasive diabetes risk prediction model based on tongue features and machine learning techniques," *International Journal of Medical Informatics*, vol. 149, no. 1, pp. 104429, 2021.
- [2] X. Huang, L. Zhuo, H. Zhang, X. Li and J. Zhang, "Lw-TISNet: Light-weight convolutional neural network incorporating attention mechanism and multiple supervision strategy for tongue image segmentation," *Sensing and Imaging*, vol. 23, no. 1, pp. 6, 2022.

- [3] M. Y. Li, D. J. Zhu, W. Xu, Y. J. Lin, K. L. Yung *et al.*, “Application of U-Net with global convolution network module in computer-aided tongue diagnosis,” *Journal of Healthcare Engineering*, vol. 2021, no. 2, pp. 1–15, 2021.
- [4] X. R. Zhang, J. Zhou, W. Sun and S. K. Jha, “A lightweight CNN based on transfer learning for COVID-19 diagnosis,” *Computers, Materials & Continua*, vol. 72, no. 1, pp. 1123–1137, 2022.
- [5] F. Bi, X. Ma, W. Chen, W. Fang, H. Chen *et al.*, “Review on video object tracking based on deep learning,” *Journal of New Media*, vol. 1, no. 2, pp. 63–74, 2019.
- [6] J. Li, X. Hu, L. Tu, L. Cui, T. Jiang *et al.*, “Diabetes tongue image classification using machine learning and deep learning,” *SSRN Journal*, 2021. <http://dx.doi.org/10.2139/ssrn.3944579>.
- [7] A. Sage, Z. Miodońska, M. Kręcichwost, J. Trzaskalik, E. Kwaśniok *et al.*, “Deep learning approach to automated segmentation of tongue in camera images for computer-aided speech diagnosis,” in *Information Technology in Biomedicine, Advances in Intelligent Systems and Computing Book Series*. Vol. 1186. Cham: Springer, pp. 41–51, 2021.
- [8] N. Guanyu, W. Caiqun, Y. Bo and P. Yong, “Tongue color classification based on convolutional neural network,” in *Future of Information and Communication Conf., Advances in Intelligent Systems and Computing Book Series*. Vol. 1364. Cham: Springer, pp. 649–662, 2021.
- [9] E. Gholami, S. K. Tabbakh and M. Kheirabadi, “Increasing the accuracy in the diagnosis of stomach cancer based on color and lint features of tongue,” *Biomedical Signal Processing and Control*, vol. 69, no. 1, pp. 102782, 2021.
- [10] Y. Tang, Y. Sun, J. Y. Chiang and X. Li, “Research on multiple-instance learning for tongue coating classification,” *IEEE Access*, vol. 9, pp. 66361–66370, 2021.
- [11] R. F. Mansour, M. M. Althobaiti and A. A. Ashour, “Internet of things and synergic deep learning based biomedical tongue color image analysis for disease diagnosis and classification,” *IEEE Access*, vol. 9, pp. 94769–94779, 2021.
- [12] T. Jiang, X. Guo, L. Tu, Z. Lu, J. Cui *et al.*, “Application of computer tongue image analysis technology in the diagnosis of NAFLD,” *Computers in Biology and Medicine*, vol. 135, no. 1, pp. 104622, 2021.
- [13] B. Yan, S. Zhang, H. Su and H. Zheng, “TCCGAN: A stacked generative adversarial network for clinical tongue images color correction,” in *2021 5th Int. Conf. on Digital Signal Processing*, Chengdu China, pp. 34–39, 2021.
- [14] S. Deepa and A. Banerjee, “Intelligent decision support model using tongue image features for healthcare monitoring of diabetes diagnosis and classification,” *Network Modeling Analysis in Health Informatics and Bioinformatics*, vol. 10, no. 1, pp. 1–16, 2021.
- [15] Y. Hu, G. We, M. Luo, P. Yang, D. Dai *et al.*, “Fully-channel regional attention network for disease-location recognition with tongue images,” *Artificial Intelligence in Medicine*, vol. 118, pp. 102110, 2021.
- [16] J. Wang, X. He, S. Faming, G. Lu, H. Cong *et al.*, “A real-time bridge crack detection method based on an improved inception-resnet-v2 structure,” *IEEE Access*, vol. 9, pp. 93209–93223, 2021.
- [17] Q. Askari, I. Younas and M. Saeed, “Political optimizer: A novel socio-inspired meta-heuristic for global optimization,” *Knowledge-Based Systems*, vol. 195, no. 5, pp. 105709, 2020.
- [18] Z. Qi, Y. Tian and Y. Shi, “Robust twin support vector machine for pattern classification,” *Pattern Recognition*, vol. 46, no. 1, pp. 305–316, 2013.
- [19] R. F. Mansour, M. M. Althobaiti and A. A. Ashour, “Internet of things and synergic deep learning based biomedical tongue color image analysis for disease diagnosis and classification,” *IEEE Access*, vol. 9, pp. 94769–94779, 2021.